A spectro-photometric model of Mars in the near-infrared

Stéphane Erard

Institut d'Astrophysique Spatiale. CNRS/Université Paris-sud

Abstract. The present model provides estimates of the spectral radiance of Mars in the 0.4-5.7 μm domain. The model is based on several composite surface spectra that correspond to the main types of materials observed. Photometric effects are simulated with both a Minnaert model and a phase function derived from ISM spectra. Aerosols scattering is taken into account for small opacities (single scattering). Thermal emission is accounted for through an emissivity model previously used to derive reflectance from IRS data. Emission and scattering by molecules are also included. Temperature and pressure are allowed to vary with season, local time, and latitude; regional effects, including surface elevation, are averaged out in this version. Results are validated by comparisons with various data sets. One of the main discrepancies with observations is related to atmospheric absorptions deeper than observed, which is probably due to coupling between absorption and scattering.

Introduction

Because it provides global compositional information on planetary surfaces and atmospheres, infrared imaging spectroscopy is considered one of the priorities for future planetary space missions. On Mars, previous low to medium resolution observations have demonstrated the power of this technics for understanding both the surface geological evolution and the atmospheric cycles. Second generation imaging spectrometers are either scheduled (OMEGA on Mars Express, VIRTIS for the Mars flyby of Rosetta) or proposed (reflight of VIRTIS) for the forthcoming Martian missions. These instruments will span the spectral range between 0.4 and 6 μm at high spatial resolution, and will observe the whole range of latitude from high-inclination orbits. The optimization of observation programs, as well as the interpretation of data, will benefit from a model of the signal to be detected. The two main purposes of such a model are 1) to provide an estimate of the signal and signal to noise ratio in given conditions, in order to set the observing modes of the instruments; 2) to provide elements of comparison so as to identify atypical measurements in the large observing data sets foreseen.

The present model is intended to simulate the signal from experiments such as OMEGA and the imaging segment of VIRTIS, which are mainly focused on surface properties. Consequently, the simulations are performed at low spectral resolution (30-60 nm spectral sampling) and do not include detailed atmospheric processes, which are barely visible in this case and are not crucial for the purpose mentioned above. The approach is to model each physical effect independently (surface reflectance, emittance and photometry, atmospheric absorption and scattering) and to combine them. The input parameters are related to the moment of observation (local time, solar longitude) and to the viewing conditions (latitude observed, emergence, phase). An important constraint is to allow very fast computing and to remain independent of spacecraft and instrument properties, such as orbital parameters or field of view. For this reason, longitudinal variations of Martian properties (temperature, pressure, albedo, retrieved from data bases) are averaged out in the input data.

Paper number 1999GL000000.
0094-8276/00/1999GL000000$05.00

Spectral types and composite spectra

Three spectral units are currently used in the model (Fig. 1). Soils are represented by two spectral types, a dark and a bright one; other types of soils exist but are not taken into account because they differ from the previous two only by subtle spectral features. Conversely, the polar caps have distinctive surface reflectance and photometric behavior, and provide a third spectral type.

The bright and dark soils spectra derive from previous integrations of ISM, IRS and telescopic spectra, respectively in Ophir Planum and Margaritifer Terra [*Erard and Calvin*, 1997]. The data are from ISM (0.81-2.45 μm), IRS (2.45-5.65 μm) and 1988 telescopic observations from [*Bell et al.*, 1990] (0.4-0.81 μm). IRS spectra are corrected from thermal emission and converted in reflectance as described in [*Erard and Calvin*, 1997]. ISM spectra are averaged within IRS footprint ($\sim$200 km wide) so the whole spectral range correspond to the same area. Telescopic and IRS spectra are convolved to $\sim$10-30 nm resolution to increase the signal to noise ratio. Atmospheric absorptions are tentatively corrected with a simple absorption model [*Erard et al.*, 1994], and the remnant features are removed by cubic spline interpolation of the continuum in order to get an estimate of the surface spectra. The gap in the ISM spectral range between 1.5 and 1.65 μm is also interpolated. The average level is then scaled to photoelectric observations of similar areas [*Roush et al.*, 1992].

The polar cap spectrum is a composite of telescopic observations from [*Clark and McCord*, 1982] (acquired on the north cap at $L_s = 209^\circ$ in 1978, used from 0.74 to 1.85 μm) and [*Bell*, 1992] (0.42-0.71 μm, acquired on the south cap at $L_s = 259^\circ$ in 1988). These data are completed above 1.85 μm with IRS spectrum M7/135 calibrated by [*Calvin*, 1990] (acquired on the south cap at $L_s = 200^\circ$). These spectra are almost the only ones of the polar caps published, therefore they are used together although only north cap spectrum includes water ice absorptions. The average level was scaled to HST radiometric measurements [*James et al.*, 1994]. Because of the low temperature ($\sim$140K) the thermal contri-

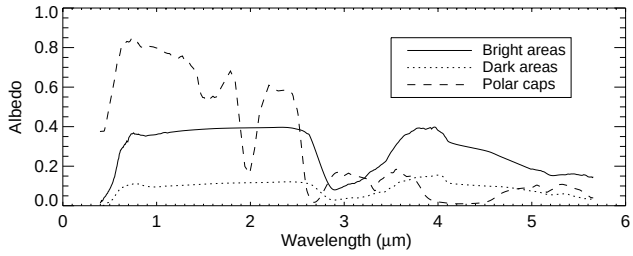

Figure 1. Normal albedo of the three types of regions included in the model. Atmospheric contributions are removed from the original data.

bution is negligible relative to the reflected sunlight, and no thermal correction is needed.

The three spectra are convolved to a common spectral resolution, and scaled as normal albedo (radiance factor at zero phase angle). Finally, scattering by aerosols and molecules is removed from the spectra to recover the surface contribution alone (see below).

Surface photometric function

Surface photometric variations are modeled with a Minnaert function:

$$r_s = B_\circ \frac{\mu_\circ^k}{\mu^{1-k}} \qquad (1)$$

where $\mu_\circ$ = cos i and μ = cos e. The two parameters $B_\circ$ (estimate albedo in normal geometry) and k (Minnaert exponent, or rate of limb darkening) depend in general on phase angle and wavelength. A specific set of parameters is used for each type of region.

The only study of the photometry of the surface alone was performed by [*Kirkland et al.*, 1997] from ISM observations between 0.8 and 2.5 μm. After removal of aerosols scattering effects, the Minnaert exponent of the surface was found to vary slightly with phase angle, but not with wavelength.

Accordingly, k is assumed independent of wavelength in the present model. Its variations with phase and albedo are estimated from a compilation of values derived from telescopic and orbital data (*eg.*, [*Binder and Jones*, 1972], [*Thorpe*, 1973], [*Pleskot and Kieffer*, 1977], [*de Grenier and Pinet*, 1995], [*Erard*, 2000]). The exponent appears to vary linearly in the 0-20° phase range, from 0.75 to 0.95 on bright regions, and from 0.55 to 0.95 on dark regions. Above 20°, the exponent remains constant with phase in all regions. On the polar cap not enough data are available to constrain the variations of the Minnaert's exponent, so the average value (k = 1.2) is used for every phase angle.

The Minnaert albedo at zero phase angle $B_\circ(0°)$ is provided by the model spectra. Its variation with phase angle is simulated with the phase function derived by [*Kirkland et al.*, 1997] on bright regions, which is the only estimate available. This function is therefore used for the three types of terrains.

All spectral dependencies of the photometric function are thus ascribed to aerosol scattering. This assumption may prove wrong in the visible range, where surface effects could be different from the NIR range.

Aerosols and Rayleigh scattering

The light scattered by airborne particles towards the observer can represent up to 25% of the signal in the NIR, even under low opacity [*Clancy and Lee*, 1991], [*Erard et al.*, 1994]. The situation modeled here is similar to that encountered during the Phobos-2 mission in 1989, and to the "low-dust scenario" of the European Mars Climate Database [*Lewis et al.*, 1999]. The aerosols contribution is accounted for by the addition of a backscattered component computed in the single-scattering approximation for a narrow particle size distribution. Using a modified gamma-distribution with effective radius and variance r_{eff}~1.25 μm and $v_{eff} = 0.25$, the scattered flux is maximum just short of 1 μm (Fig. 2). A simple Mie scattering code was used in the computation, therefore assuming spherical particles, and the complex refraction index is kept constant in the whole spectral domain; this approximation is not so severe in the 0.3-2.6 μm region where scattering is largest. The underlying assumption is that extinction is nearly compensated by forward scattering. This assumption is valid at opposition in the Martian conditions, but degrades with increasing emergence and incidence angles. In spite of these approximations, the resulting spectrum provided a good fit to various ISM estimates of the scattered contribution [*Drossart et al.*, 1991] [*Erard et al.*, 1994], and was also found consistent with observations by other instruments on board the Phobos-2 spacecraft [*Chassefiere et al.,*, 1995]. This aerosol contribution is scaled to yield an opacity of 0.2 at 1.9 μm, and is added to the surface radiance:

$$r_a \;=\; Q_{back}\;\frac{\tau_0(\lambda_0)}{Q_{ext}(\lambda_0)}\;f(\varphi = 0^\circ) \qquad (2)$$

where τ_0 (λ_0) is the reference opacity at $\lambda_0 = 1.9$ μm, Q_{back} and Q_{ext} are the coefficients for backscattering and extinction, and f(φ) is the aerosol phase function (also computed from Mie theory). The backscattered spectrum is shown in Fig. 2, and Fig. 3 depicts its variation with phase angle. The trend observed in Fig. 3 is related to the diminution of the rear lobe and to the rapid elongation of the front lobe with increasing wavelength for the average particle size used here. The approximation of spherical particles apparently breaks for phase angles larger than ~160°, where it yields an unreasonably large contribution (> 10 times the backscattered flux); this may be related to the strong dependence of forward scattering on particle shape.

Rayleigh scattering by CO_2 molecules is also taken into account. This contribution r_{Rayl} becomes important at short wavelength near the limb (large emergence) and reduces the surface contrast in blue light. Overall, the re-

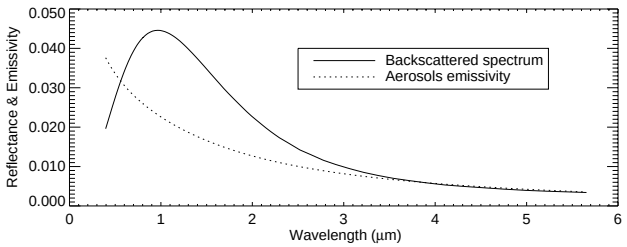

Figure 2. Aerosols spectral properties for the size distribution and indices used in the model.

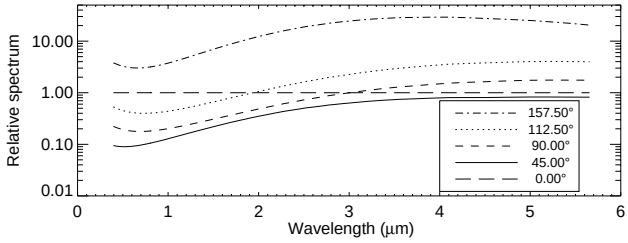

Figure 3. Aerosols scattered spectrum under various phase angles. All spectra are divided by the backscattered spectrum (at 0° phase angle).

flected component writes:

$$L_{\lambda,r}(i,e,\varphi) = \left[r_s(i,e,\varphi)A(\mu_\circ,\mu) + r_a \frac{f(\varphi)}{\mu f(0^\circ)} A'(\mu_\circ,\mu) + r_{Rayl}(i,e)\frac{f_{Rayl}(\varphi)}{\mu} \right] \frac{E_S}{\pi R^2} \quad (3)$$

where $E_S(\lambda)/R^2$ is the solar irradiance at Mars distance (W m^2 μm^{-1}). The atmospheric transmission $A(\mu_\circ,\mu)$ is simulated using a synthetic spectrum computed with MODTRAN for 6 mbar of CO_2 and a standard thermal profile. CO and H_2O, which produce only minor absorptions in this range, are not included in the model. The actual transmission is scaled according to surface pressure and to the atmospheric path, and so is Rayleigh scattering. Although any value can be entered, the default surface pressure is the daily average at the reference level, with variations in solar longitude and latitude. These variations are retrieved from the European Mars Climate Database, in the low dust scenario [*Lewis et al.*, 1999], [*Forget et al.*, 1999], [http://gurtu.lmd.jussieu.fr/mars/]. The atmospheric layer above the aerosols A'($\mu_\circ$, μ) is assumed to have a pressure half that at the surface (i.e., aerosols are located 6-8 km above the surface).

Thermal contributions

The emitted fluxes are added to the reflected light, and dominate the signal above ∼4 μm. These contributions are computed as:

$$L_{\lambda,e}(e,\varphi) = \varepsilon_s(\mu)A(\mu)B_\lambda(T_S) + \left[1 - A(\mu) + \frac{\varepsilon_a}{\mu}A'(\mu)\right] B_\lambda(T_A) \quad (4)$$

where the two terms are respectively the surface emission, and the emission of the gaseous atmosphere and the aerosols. B_λ is the black body radiance at temperature T. The emissivity of the atmosphere [1 - A(μ)] is the estimate for a single isothermal layer with no scattering. Aerosols emissivity ε_a is the absorption coefficient scaled in a similar way as the backscattered spectrum (Fig. 2).

The directional emissivity of the surface $\varepsilon_s(\mu)$ is here approximated as 1-p_N, where p_N is the normal albedo (input spectrum for each region). The underlying assumption is that of a Lambertian behavior in the thermal range, and is accurate within ∼10-20%. This model is consistent with that used to remove thermal emission from the input spectra at high wavelength.

Temperatures are sampled from the European Mars Climate Database in solar longitude, local time and latitude, and are averaged in longitude, so that variations with altitude are not accounted for. A single average temperature is used for the atmosphere, corresponding to the layer 5 to 8 km above the datum. This value is assumed to be the temperature of the aerosols. Using a thermal profile to compute the atmospheric contribution would provide much better accuracy, but would require much longer computation times.

Discussion

The model is currently valid for low opacities (∼0.2-0.5), moderated phase angles (< 160°), and low surface elevations (< 3 km), including night-time observations. The polar cap radiance is computed only when a polar cap is visible, according to standard recession curves.

The model is validated by comparison with various observations: ISM, IRS (newly restored data by [*Kirkland et al.*, 1999]), HST, and telescopic spectra. In all cases, the shape and level of the continuum are consistent with observations, except on dark areas above 4 μm at mid-day, where the level may be underestimated by a factor of ∼2; this is partly due to the averaging of the GCM temperatures in input. The main CO_2 bands (at 2.7 and 4.2 μm) are often deeper than observed at this spectral resolution, which is probably related to coupling between absorption and scattering, but their variations are also consistent. At short wavelengths, simulations of Earth-based observations show the same behavior which is observed *eg.* on the 1995 and 1997 HST images (Fig. 4): bright terrains can be much brighter than the polar caps above 0.65 μm (due to the different photometric functions) but not in the visible; dark regions are always a factor of 1.5 to 3 darker than bright ones, except in blue light where surface contrast almost vanishes, especially at the limb; Mie scattering can represent up to 50% of the flux at the limb, which is probably exaggerated (the aerosols model breaks down for large angles). On the night side, the estimated radiance is only half what was observed by IRS, which can be explained either by large scattering in the atmosphere, or by stray light in the instrument.

The model appears to simulate the Martian spectrum rather well inside its domain of validity: moderate viewing angles (<65°), low opacity ($\tau \sim 0.2$), low surface elevation. In its present state, it is a useful tool to prepare an observ-

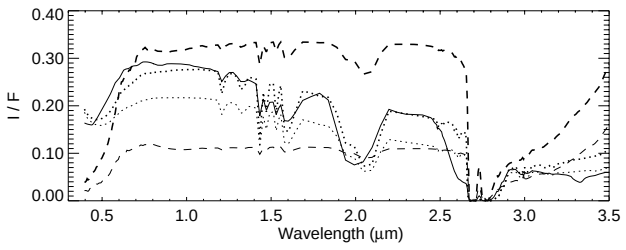

Figure 4. Simulation of Earth-based observations during a perihelic opposition (phase angle 10°): south polar cap (solid line, i and e ∼70°), disk center (dashed lines, i and e ∼5°), high summer (N) latitudes (dotted lines, i and e ∼80°). Bold lines correspond to bright regions. All regions are observed at noon. The level is the overall flux divided by the incident solar flux.

ing program. However, improvements are required to perform detail comparisons with orbital observations, and include: use of temperature/pressure maps from GCM rather than longitudinal averages, use of a radiative transfer code to simulate large opacities and large viewing angles, use of an atmospheric model to simulate the aerosols contribution above the volcanoes, and addition of water clouds in the atmosphere.

Acknowledgments. This work was partially supported by the French Programme National de Planétologie. Thanks to E. Palomba for computing the synthetic atmospheric spectrum, to P. Drossart and F. Forget for constructive discussions regarding the scattering code and the Mars Climate Database, to E. Lellouch and two anonymous reviewers who helped improving the manuscript. An online version of this model will be available at IAS Planetary Data Center (http://www.ias.fr/cdp/).

References

Bell, J., Charge-coupled device imaging spectroscopy of Mars 2. Results and implications for Martian ferric mineralogy, *Icarus, 100,* 575-597, 1992.

Bell, J.F., T.B. McCord, and P.G. Lucey, Imaging spectroscopy of Mars (0.4-1.1 m) during the 1988 opposition, *Proc. Lunar and Planet. Sc. Conf., 20,* 479-486, 1990.

Binder, A.B., and J.C. Jones, Spectrophotometric studies of photometric function, composition, and distribution of the surface materials of Mars, *J. Geophys. Res., 77,* 3005-3020, 1972.

Calvin, W., Additions and corrections to the absorption coefficients of CO2 ice: application to the Martian south polar cap, *J. Geophys. Res., 95,* 14743-14750, 1990.

Chassefière, E., P. Drossart, and O. Korablev, Post-Phobos model for the altitude and size distribution of dust in the low Martian atmosphere, *J. Geophys. Res., 100,* 5525-5539, 1995.

Clancy, R.T., and S.W. Lee, A new look at dust and clouds in the Mars atmosphere: Analysis of emission-phase-function sequences from global Viking IRTM observations., *Icarus, 93,* 135-158, 1991.

Clark, R.N., and T.B. McCord, Mars residual polar cap: Earth-based spectroscopic confirmation of water ice as a major constituent and evidence for hydrated minerals, *J. Geophys. Res., 87,* 367-370, 1982.

de Grenier, M., and P. Pinet, Near-opposition Martian limb-darkening: quantification and implication for visible-near-infrared bidirectional reflectance studies, *Icarus, 115,* 354-368, 1995.

Drossart, P., J. Rosenqvist, S. Erard, Y. Langevin, J.-P. Bibring, and M. Combes, Martian aerosols properties from the Phobos/ISM experiment, *Annales Geophysicae, 9,* 754-760, 1991.

Erard, S., The 1994-95 apparition of Mars observed from Pic-du-Midi, *Planet. Space Sc., 48,* 1271-1287, 2000.

Erard, S., and W. Calvin, New composite spectra of Mars, 0.4-5.7m, *Icarus, 130,* 449-460, 1997.

Erard, S., J. Mustard, S. Murchie, J.-P. Bibring, P. Cerroni, and A. Coradini, Effects of aerosols scattering on near-infrared observations of the Martian surface, *Icarus, 111,* 317-337, 1994.

Forget, F., F. Hourdin, R. Fournier, C. Hourdin, O. Talagrand, M. Collins, S. Lewis, P. Read, and J.-P. Huot, Improved general circulation models of the Martian atmosphere from the surface to above 80 km, *J. Geophys. Res., 104,* 24,155-24,176, 1999.

James, P.B., R.T. Clancy, S.W. Lee, L.J. Martin, R.B. Singer, E. Smith, R.A. Kahn, and R.W. Zurek, Monitoring Mars with the Hubble Space Telescope: 1990-1991 observations, *Icarus, 109,* 79-101, 1994.

Kirkland, L., A. Treiman, and S. Murchie, Photometry of bright regions on Mars: ISM results (abstract), *LPSC XXVIII,* 729-730, 1997.

Kirkland, L.E., K.C. Herr, P.B. Forney, and J.W. Salisbury, 1969 Mariner 7 Infrared Spectrometer: Data recovery and comparison to TES (abstract), *LPSC XXX,* abstract #1693, 1999.

Lewis, S.R., M. Collins, P.L. Read, F. Forget, F. Hourdin, R. Fournier, C. Hourdin, O. Talagrand, and J.-P. Huot, A Climate Database for Mars, *J. Geophys. Res., 104,* 24,177-24,194, 1999.

Pleskot, L.K., and H.H. Kieffer, The infrared photometric function of Mars and its bolometric albedo, *Icarus, 30,* 341-359, 1977.

Roush, T., E. Roush, R. Singer, and P. Lucey, Estimates of absolute flux and radiance factor of localized regions of Mars in the (2-4μm) wavelength region, *Icarus, 99,* 42-50, 1992.

Thorpe, T.E., Mariner 9 photometric observations of Mars from November 1971 through March 1972, *Icarus, 20,* 482-489, 1973.

S. Erard, IAS bât.121, Université Paris-11, 91405 Orsay campus, France. (e-mail: erard@ias.fr)

(Received September 18, 2000; revised January 2, 2001;
accepted January 8, 2001.)